1.0

2.6 2.5

3.2 2.2

2.0

1.1

1.8

1.25 1.4 1.6

AD A096765

AFWAL-TR-80-2125
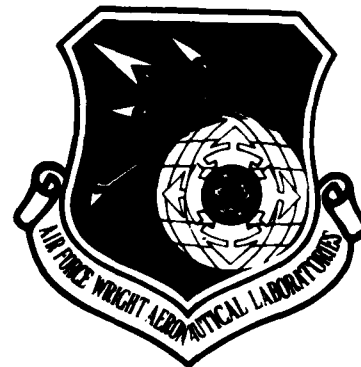
AN INVESTIGATION OF SLURRY FUEL COMBUSTION

G. A. Szekely and G. M. Faeth

The Pennsylvania State University
Department of Mechanical Engineering
University Park, PA 16802

January 1981

TECHNICAL REPORT AFWAL-TR-80-2125
Final Report for Period November 1979 - October 1980

DTIC FILE COPY

81 3 24 017

This technical report has been reviewed and is approved for publication.

ALVIN F. BOPP
Fuels Branch, Fuels and Lub Div
Aero Propulsion Laboratory

ARTHUR V. CHURCHILL
Chief, Fuels Branch
Fuels and Lubrication Division
Aero Propulsion Laboratory

FOR THE COMMANDER

BENITO P. BOTTERI, Asst Chief
Fuels and Lubrication Division
Aero Propulsion Laboratory

AIR FORCE/56780/18 March 1981 — 100

REPORT DOCUMENTATION PAGE		READ INSTRUCTIONS BEFORE COMPLETING FORM
1. REPORT NUMBER AFWAL-TR-80-2125	2. GOVT ACCESSION NO. AD-A096 765	3. RECIPIENT'S CATALOG NUMBER
4. TITLE (and Subtitle) An Investigation of Slurry Fuel Combustion		5. TYPE OF REPORT & PERIOD COVERED Final Report, Nov 79 - Oct 1980
		6. PERFORMING ORG. REPORT NUMBER
7. AUTHOR(s) G. A. Szekely and G. M. Faeth		8. CONTRACT OR GRANT NUMBER(s) F33615-77-C-2004
9. PERFORMING ORGANIZATION NAME AND ADDRESS The Pennsylvania State University Department of Mechanical Engineering University Park, PA 16802		10. PROGRAM ELEMENT, PROJECT, TASK AREA & WORK UNIT NUMBERS 30480591 62203F
11. CONTROLLING OFFICE NAME AND ADDRESS Air Force Wright Aeronautical Laboratories AFWAL/POSF Wright-Patterson AFB OH 45433		12. REPORT DATE January 1981
		13. NUMBER OF PAGES 42
14. MONITORING AGENCY NAME & ADDRESS(if different from Controlling Office)		15. SECURITY CLASS. (of this report) Unclassified
		15a. DECLASSIFICATION DOWNGRADING SCHEDULE

16. DISTRIBUTION STATEMENT (of this Report)

Approved For Public Release; Distribution Unlimited

17. DISTRIBUTION STATEMENT (of the abstract entered in Block 20, if different from Report)

18. SUPPLEMENTARY NOTES

19. KEY WORDS (Continue on reverse side if necessary and identify by block number)

Carbon Slurry   Slurry Combustion
High Density Fuels   Carbon Combustion
Slurry Fuels

20. ABSTRACT (Continue on reverse side if necessary and identify by block number) A theoretical and experimental investigation of the combustion properties of carbon slurry fuels was performed. This involved observing the combustion of individual drops (400-1000 μm in diameter) supported at various positions within an open, turbulent diffusion flame. When a slurry drop was exposed to the flame, the liquid fuel in the slurry evaporated in the first stage, leaving a carbon agglomerate consisting of all the carbon particles originally in the slurry. The second stage of the process involved heat-up and reaction of the agglomerate (Continued on reverse)

DD FORM 1473 1 JAN 73   EDITION OF 1 NOV 65 IS OBSOLETE

Block 20 - ABSTRACT

Consumption of the agglomerate was the slowest step in the process, requiring 90-95 percent of the lifetime of the particle, even in regions where agglomerate reaction was fast. An analysis was developed to provide predictions of agglomerate reaction rates and lifetimes. The model was tested with measurements in the lean portions of the flame (equivalence ratios in the range 0.272-0.778). Good agreement between predictions and measurements was observed in this region, with respect to both particle temperature and size variations. Use of a catalyzed slurry was found to increase burning rates and extend the lean limit for agglomerate reaction. It is recommended that further testing and model development be undertaken, considering combustion properties at higher equivalence ratios and for drops more representative of the sizes encountered in combustion chambers. The model should also be extended to consider the liquid gasification stage of slurry combustion.

PREFACE

Accession For
NTIS GRA&I
DTIC TAB
Unannounced
Justification

By
Distribution/
Availability Codes
Avail and/or
Special
Dist

A

TABLE OF CONTENTS

LIST OF ILLUSTRATIONS

LIST OF TABLES

Nomenclature

Symbol	Description
a_i	area/reactivity factor, Eq. (34)
A_i	preexponential factor
C_p	specific heat
d	injector diameter
D	effective binary diffusivity
D_{ij}	binary diffusivity
E	activation energy
h	enthalpy
h_f^o	enthalpy of formation
k'	Boltzman constant
K	dimensionless mass burning rate, Eq. (16)
K_i	equilibrium constant
Le	Lewis number
m_i''	mass flux of species i
m_p''	mass flux at particle surface
M	mixture molecular weight
M_i	molecular weight of species i
p	mixture pressure
p_i	partial pressure of species i
q_c''	convective heat flux at particle surface
q_r''	radiative heat flux at particle surface
r	radial distance
R	Universal gas constant

Nomenclature (Continued)

Symbol	Description
R_i	reaction rate of species i
t	time
T	temperature
u	gas velocity surrounding particle
v	radial velocity
x	distance from injector
x_i	mole fraction of species i
Y_i	mass fraction of species i
$\tilde{Y}_i$	mass fraction of element i
α	average property factor, Eq. (A-1)
γ	radius ratio, Eq. (15)
δ	radius ratio, Eq. (14)
ϵ	surface emissivity
ϵ'	Lennard-Jones characteristic energy
θ	generic property
λ	thermal conductivity
μ	viscosity
ν_{ij}	stoichiometry factor, Eq. (4)
ξ	dimensionless radius, Eq. (13)
ρ	density
σ	Stefan-Boltzman constant
σ'	Lennard-Jones characteristic length
ϕ	equivalence ratio
ϕ_{ij}	property factor, Eq. (A-3)

Nomenclature (Continued)

Subscripts	Description
c	combustion products
p	particle surface
ref	reference state
s	solid
w	room surfaces
o	initial condition
∞	ambient state for concentrations
∞_T	ambient state for temperature

Summary

The results of a brief preliminary study of the combustion
properties of carbon slurry fuels are reported. The carbon slurry
fuels were formulated by mixing noncatalyzed and/or catalyzed medium
thermal carbon black (roughly 50 percent by weight) with JP-10.

The combustion of individual supported slurry drops, 400-1000 μm
initial diameter, was observed in an open turbulent diffusion flame
at atmospheric pressure. The environment of the drops within the
flame was known from measurements of mean velocity, temperature and
composition. The drops were supported on the junction of a thermo-
couple. Shadowgraph motion pictures were also obtained for the
process. This data provided the variation of particle temperature
and diameter as a function of time.

A two-stage combustion process was observed. The first stage
involved heat-up and evaporation of the liquid, leaving a solid
agglomerate of the carbon particles in the slurry. The second
stage involved heat-up and reaction or quenching of the agglomerate.

A model was constructed for the second stage of the process. This
involved analysis of heat and mass transfer processes in the convective
environment surrounding the agglomerate, and the chemical reaction of
carbon with oxygen, carbon dioxide, and water vapor at the surface
of the particle. Radiative heat transfer between the agglomerate and
its surroundings was also considered. The predictions of the model
were compared with measurements in the lean portions of the flame
(equivalence ratios in the range 0.272-0.778).

The major findings of the study can be summarized as follows:

1. For present test conditions, all the solid carbon in the
    slurry remained in the agglomerate and heat-up and reaction
    of the agglomerate dominated the lifetime of the particle--
    usually requiring 90-95 percent of the particle lifetime,
    even in locations where agglomerate reaction was nearly
    diffusion controlled.

2. While liquid heat-up and gasification occurs in all regions
    of the flame, agglomerate reaction was limited to regions
    with equivalence ratios in the range 0.37-4.0 for noncatalyzed
    slurries and 0.21-4.0 for catalyzed slurries. The carbon
    reaction was quenched at other locations.

3. The model yielded good predictions of agglomerate reaction
    rates in the range tested (equivalence ratios of 0.272-0.778,
    where the main reactant is oxygen). Conditions near both the
    diffusion and reaction rate controlled limits were included
    in the comparison. This agreement was obtained by selecting a
    single empirical, area/reactivity multiplication factor, which
    allows for the pore and surface structure of the carbon ag-
    glomerate and the effect of a catalyst.

4. The model yielded good predictions of agglomerate-life-
   histories over the same range of conditions. Reasonable
   predictions of heat-up times and particle temperatures
   indicate that the thermal aspects of the model are adequate
   over the present test range.

5. Adding catalyst increased agglomerate burning rates, for
   conditions not too near the diffusion controlled limit.
   This effect could be treated in the theory by selecting
   a higher area/reactivity multiplication factor for the
   catalyzed slurry. The presence of catalyst also extended
   the lean limit for quenching.

6. Some particle shattering was observed with catalyzed
   slurries in the lean region of the flame.

These conclusions are based on test results with relatively large
particles, 400-1000 μm in diameter. In particular, the effect of pore
diffusion is likely to vary with particle size. Therefore, the area/
reactivity multiplication factors selected to correlate the present
data are not considered to be appropriate for other test conditions,
without further testing. The effect of pressure and combustion
properties in the fuel rich region (equivalence ratios of 0.778-4.0)
were also not assessed in this study. This implies considerable
uncertainty concerning agglomerate reaction with carbon dioxide,
water vapor, and other species present at high equivalence ratios. In
order to remove these uncertainties, it is recommended that additional
work be undertaken using particle sizes more representative of com-
bustion chamber conditions, as well as test environments extending
to richer mixture ratios.

1. Introduction

1.1 General Objectives

The propulsion system of airbreathing missiles is frequently volume limited. This implies that the volume of the propulsion system is a critical factor in determining missile range and performance—as opposed to propulsion system weight. Since fuel volume comprises a significant fraction of propulsion system volume, fuels that have a large chemical energy release per unit volume (high volumetric energy density) are particularly attractive for such applications.

There has been continuous development of high volumetric energy density liquid fuels to meet these needs [1].* However, it has become increasingly difficult to achieve further improvements using liquids alone. This has resulted in increased consideration of slurries, since these fuels can be handled and burned similar to liquids and yet have increased density due to the presence of solids [2-5]. The objective of the present investigation was to conduct a preliminary investigation of the combustion properties of carbon slurry fuels of interest to the Air Force [2,3].

The carbon slurry fuels considered in this investigation were formulated by Suntech, Inc., Marcus Hook, PA, for use during combustor tests by the AiResearch Manufacturing Company of Arizona [2,3]. While these fuels are representative of candidate carbon slurry fuels, they do not necessarily represent the most attractive formulations since fuel development efforts are still in progress. Nevertheless, the materials should still provide a reasonable indication of carbon slurry combustion properties, useful for subsequent fuel development efforts.

The properties of the fuel considered during the present investigation are summarized in Table 1. The fuels consist of a medium thermal carbon black, with JP-10 as the liquid fuel. Two slurries were tested, each containing roughly 50% carbon by weight. The ultimate carbon particle size was 0.3 μm. One slurry was catalyzed with a proprietary lead compound.

The overall combustion characteristics of carbon slurry fuels have been examined in gas turbine combustors [3], and in well-stirred reactors [5]. The objective of the present investigation was to examine slurry combustion on a more fundamental level, by observing the combustion of individual slurry drops. The experimental technique involved observations of single slurry drops (400-1000 μm in diameter). The drops were supported at various positions within a turbulent diffusion flame in order to provide an environment representative of actual combustion chamber conditions. Measurments were made of the variation of particle diameter and temperature as a function of time. The process was also modeled theoretically and predictions and measurements were compared.

---

*Numbers in brackets denote references.

Table 1

Properties of the Carbon Slurry Fuels[a]

	Noncatalyzed	Catalyzed[b]
Designation	790-928	790-942
Liquid	JP-10	JP-10
Dispersed Carbon[c] (wt %)	50.4	49.2

[a] Fuels supplied by R. S. Stearns, Suntech, Inc.,
P. O. Box 1135, Marcus Hook, PA 19061.

[b] The catalyst is a proprietary lead compound [6].

[c] The dispersed carbon is a medium thermal carbon (carbon
black) having an ultimate particle size of 0.3 μm.
Further properties of this material are provided in
Ref. 2.

1.2 Previous Studies

The present study is an extension of earlier work in this laboratory [3,4]. The test fuel and many aspects of the experiments are similar. The general test procedure involved observations of slurry drops supported in an open turbulent diffusion flame.

The major findings of Ref. 4 are as follows:

1. The combustion of a slurry drop occurred in four stages: 1) heat-up of the drop and, at times, ignition of liquid fuel vapors; 2) evaporation or combustion of the liquid fuel accompanied by agglomeration of the carbon particles in the slurry; 3) further heating of the carbon agglomerate once all the liquid has evaporated; and 4) fragmentation, reaction or quenching of the agglomerate.

2. Combustion of the carbon agglomerate only occurred over a limited equivalence ratio range (0.21-4 for the catalyzed slurry, 0.37-4 for the noncatalyzed slurry).

3. Even in regions where the carbon agglomerate reacted, the heat-up and reaction of the agglomerate was the slowest step in the combustion process, generally requiring 20 times longer than the time required to gasify the liquid.

Figure 1 is a scanning electron microscope photograph of the surface of a partly reacted agglomerate. The light areas on the photograph are the surface of the solid agglomerate, the dark areas represent pores. The agglomerate is clearly very porous, with the carbon surface area available for reaction much greater than the apparent outer surface area of the agglomerate.

These general observations concerning the combustion properties of carbon agglomerates are similar to results found for coal slurries [7,8]. In the case of coal, however, the presence of ash and volatile material in the coal, materially influences the details of the process.

1.3 Specific Objectives

Previous investigations have demonstrated the importance of agglomerate formation and reaction during the combustion of carbon slurries. Some information concerning the regions of flames where agglomerates react has also been generated. However, existing data on agglomerate reaction rates are very limited. Furthermore, no attempt to model the agglomerate reaction process has been reported.

With this status in mind, this investigation extended the results of Refs. 3 and 4, employing a similar experimental arrangement. The specific objectives of the study were as follows:

Figure 1.   SEM photograph of agglomerate from a catalyzed slurry drop in the glowing region, . x'd   459 (magnification   25000) [4].

i. Complete additional measurements of the variation of
    particle size and temperature with time for drops sup-
    ported at various positions within a turbulent diffusion
    flame. In particular, generate more complete information
    on agglomerate burning rates as a function of position in
    the flame.

ii. Formulate a model for the reaction of the carbon agglom-
    erate, using existing information on carbon reaction
    rates. Employ the model to compute agglomerate-life-
    histories and compare predictions and measurements.

The supported particles used during this investigation had diameters
in the range 400-1000 μm, which is much larger than typical combustor
applications. For preliminary work, however, this approach had ad-
vantages since more detailed measurements can be made with large
particles, helping to provide more insight concerning slurry combustion
properties.

2. Test Arrangement

2.1 Apparatus

The test apparatus involved modification of an earlier arrangement
employed for a study of gas and spray diffusion flames [9,10]. A sketch
of the modified apparatus appears in Fig. 2. The arrangement consists of
an injector flowing propane gas, which is burned as a diffusion flame
in stagnant room air. The test drop is supported from either a thermo-
couple or a quartz probe at various locations in the flame. The drops
are also photographed with a motion picture camera, as shadowgraphs.

The propane gas injector was positioned near the bottom of the test
stand and oriented vertically upward. The test stand was an area 1.2 mm
square and 3 m high enclosed with a single thickness of 16 mesh screen.
The test stand was located within a room having dimensions 4m x 7m x 4m
high. Combustion products were removed through an exhaust fan located
near the ceiling of the test cell. The injector was seated on a support
which allowed a vertical movement of 1.2 m. Two traversing mechanisms
were used to position the nozzle in the horizontal plane.

The nozzle was a full-cone air atomizing injector, with no swirl,
manufactured by the Spraying Systems Company (Model 1/4 J 2050 fluid
nozzle and Model 67147 air nozzle). The outlet diameter of the nozzle
was 1.194 mm.

The gas flame was stabilized near the exit of the injector using an
array of four hydrogen capillary flames. The flame tubes were mounted
in a symmetrically opposed pattern injecting toward the centerline of
the injector passage. The flow passages for the hydrogen were slots
0.4 mm wide and 2 mm long, with the long axis parallel to the injector
centerline. The lower edges of the slots were 1.8 mm above the face of
the injector. The exit planes of the slots were 6.4 mm apart.

MOTION PICTURE
CAMERA

FUEL DROP

PROBE

FLAME

ARC LAMP

SHIELD

PNEUMATIC CYLINDER

PNEUMATIC VALVE

HYDROGEN PILOT
FLAMES

INJECTOR

AIR SUPPLY

PROPANE SUPPLY

HYDROGEN SUPPLY
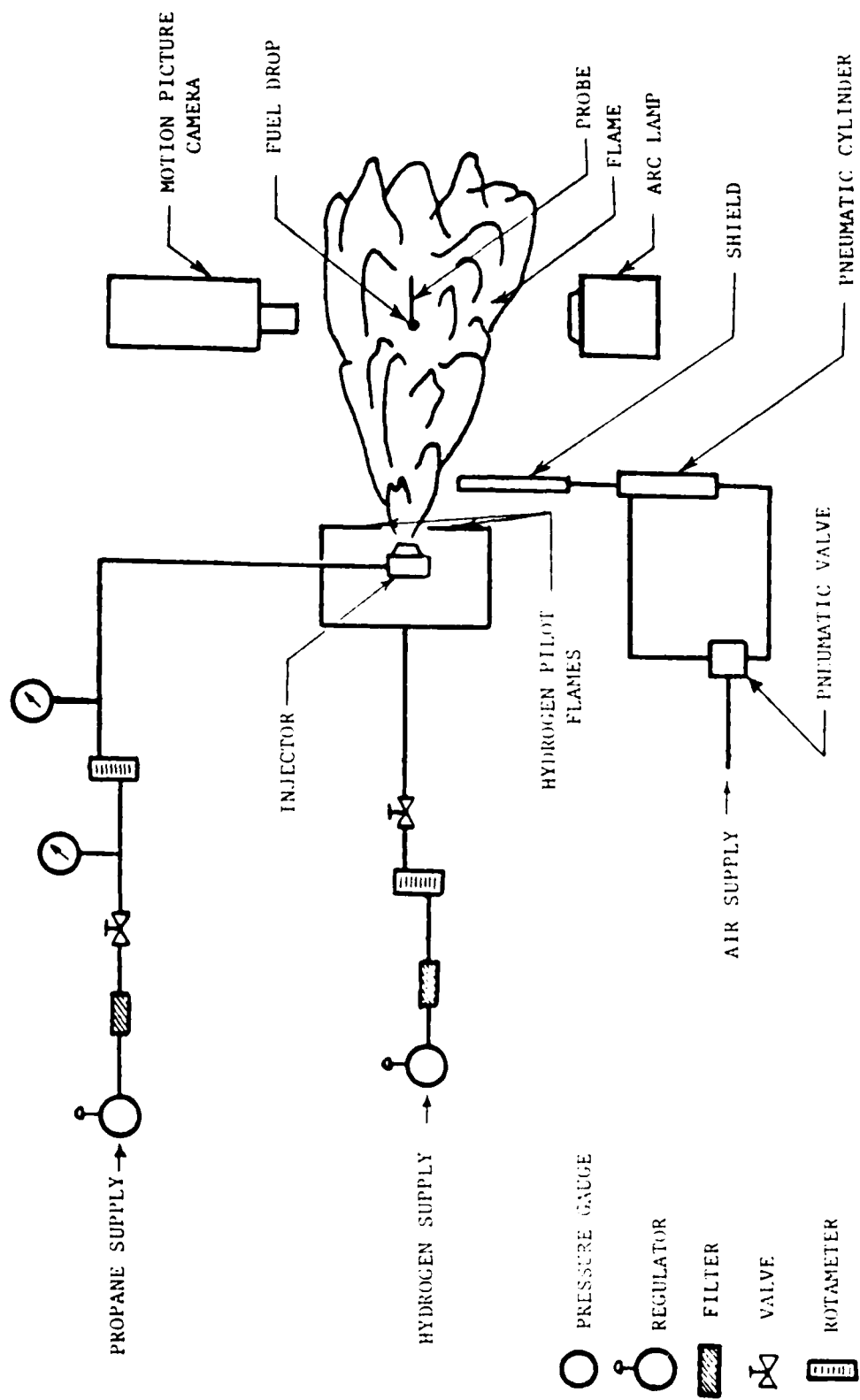
PRESSURE GAUGE

REGULATOR

FILTER

VALVE

ROTAMETER

Figure 2. Sketch of the test apparatus.

6

The propane gas flow rate was metered with a Matheson Model 604 rotameter and controlled by a Harris Model 2515 pressure regulator with an output capacity of 0-0.69 MPa. The flow rate of the hydrogen gas was metered with a Matheson Model 601 rotometer and controlled with a Matheson Model 1H pressure regulator having an 0-1.38 MPa output capacity. The rotameters for both the propane and hydrogen flows were calibrated with a Precision Scientific Company wet-test meter (2.83 ml/rev).

The fuel drops were mounted with a hypodermic needle. The flame was deflected from the mount region until the droplet was in place. The deflector was constructed from a 200 x 305 mm sheet of stainless steel, having a thickness of 3 mm. The drop combustion process was initiated by removing the deflector with a pneumatic cylinder arrangement.

2.2   Instrumentation

2.2.1   Drop Environment Measurements

The drop environment at each test location within the flame was measured. This involved measurements of mean velocity, temperature and composition. Mean velocities were measured with a laser-Doppler anemometer, which employs frequency shifting so that flow reversals could be detected. Mean temperature was measured with a 50 μm diameter platinum/platinum-10% rhodium thermocouple (with a radiation error of less than 35°C over the test range). Mean concentrations were measured by extracting gas samples isokinetically and analyzing them with a gas chromatograph. The details of these techniques are presented elsewhere [9,10].

2.2.2   Drop Measurements

The drop combustion process was observed with a 16 mm, Photosonics, Model 16-B, motion picture camera. The camera optics provided a 2:1 magnification. The camera was powered with a Kepco, SM 36-5 AM d.c. power supply. The film speed was indicated with a timing light on the camera, activated with an Adtrol Electronic pulse generator, Model 501. Kodak Plus-X reversal film was used for all tests.

Backlighting for shadowgraph measurements was provided by a Pek, Model 401A, 75W mercury arc lamp. The light from the arc was collimated and directed toward the drop location. A diffuser screen was employed behind the drop to equalize the light intensity of the background. The background intensity was adjusted so that envelope flames around the drop could also be observed.

The film records were analyzed on a frame by frame basis, using a Vanguard motion picture analyzer. Photographs of objects of known size at the drop location provided a calibration of distances on the film.

Particle temperatures were measured by mounting the test drop at the junction of a thermocouple. A Pt/Pt-10% Rh thermocouple was used, constructed of 75 μm diameter wires. In order to help support the drop, the junction was placed within a round bead, formed with Sauereisen cement (300-400 μm in diameter). The output of the particle thermocouple was recorded digitally on a Nicolet Explorer Oscilloscope, Model 206, and reduced to temperature-time data on a computer.

2.3 Test Conditions

Tests were conducted using the burner operating condition summarized in Table 2. The drops were mounted along the centerline of the flow. Relatively complete structure measurements have been reported for this flame, as noted earlier [9]. Details of interest to this investigation will be discussed later.

3. Theoretical Considerations

3.1 Description of the Model

Results obtained during this and earlier investigations indicate that slurry drop combustion is primarily a two-stage process involving gasification of liquid in the first stage and heat-up and reaction of the agglomerate in the second stage. Since the agglomerate does not actively participate in the first stage, other than influencing the density of the particle, it is convenient to treat these two stages separately.

The following analysis will be limited to the second stage--involving heat-up and reaction of the agglomerate. The present investigation emphasized this aspect of the problem since reaction of the agglomerate is the slowest step in the process. Therefore, agglomerate reaction generally controls combustor performance. Furthermore, agglomerate reaction presents the greatest uncertainties; in contrast, gasification of liquid drops is reasonably well understood [11].

The initial condition of the present analysis is the point where all the liquid has vaporized and the agglomerate is at the wet-bulb temperature appropriate for liquid vaporization (the wet-bulb temperature is slightly below the boiling temperature of the liquid for a pure fuel like JP-10 [11]). The objective of the analysis is to predict the subsequent heat-up and reaction of the agglomerate. This involves determining the variation of particle temperature and diameter as a function of time.

3.2 Agglomerate Reaction Model

Since the test droplets were supported at fixed locations, the motion of the particle is not considered. The formulation was limited to determining the rate of consumption of carbon in the

8

Table 2

Burner Flame Characteristics[a]

Fuel:	propane
Fuel flow rate:	176 mg/s
Initial fuel jet velocity:	88.7 m/s
Initial fuel jet diameter:	1.194 mm
Jet Reynolds number:	23600
Orientation:	vertical (upward)
Flame Height:	460 mm (visual)
Injector Thrust:	15.6 mN
Hydrogen flow rate:	0.126 mg/s
Ambient and injector inlet temperature:	296 K
Ambient pressure:	97 kPa

[a]Nozzle is Spraying Systems Co. Model 1/4 J 2050 fluid nozzle and
Model 67147 air nozzle, air atomizing injector.

agglomerate, the rate of heat transfer to the particle, and the rate of chemical energy release at the surface of the particle.

A sketch of the model appears in Fig. 3. The major assumptions of the analysis are as follows:

1. The particle is assumed to be spherical and particle spacing is large so that the surroundings can be taken as an infinite medium having uniform properties.

2. The gas flow field around the particle is assumed to be quasisteady, i.e., the flow field has properties equivalent to a steady state flow field, for the same boundary conditions, at each instant of time.

3. Flow fields around spheres are too complex to analyze exactly; therefore, the conventional film theory approximation is employed to represent the effect of convection [11]. This assumption implies that gas phase transport processes can be represented as a spherically symmetric flow through a stagnant layer whose outer boundary is fixed empirically.

4. The particle is assumed to consist of pure carbon and has a uniform temperature at each instant of time.

5. Solid carbon is only assumed to react at the apparent surface of the particle. The effect of pores and reaction within the particle is treated by introducing an empirical area/reactivity multiplication factor. Reaction of solid carbon with oxygen, carbon dioxide, and water vapor is considered.

6. The gases surrounding the particle are assumed to be represented by their mean properties and the effect of turbulent fluctuations is ignored. The actual gas mixture was approximated by oxygen, nitrogen, carbon dioxide, carbon monoxide, water vapor, hydrogen and hydroxyl radicals--in thermodynamic equilibrium.

7. Only concentration diffusion is considered, employing an effective binary diffusion coefficient for all diffusing species. All species are assumed to have equal specific heats (assumed constant) and molecular weights, for the purpose of computing diffusion and energy transport rates in the flow. Constant average values are used for all properties in the gas phase.

8. The gas is assumed to be transparent to radiation, however, provision is made for particle radiation to the confinement surrounding the flow.

9. The pressure within the flow field is assumed to be constant.

10. The gases maintain thermodynamic equilibrium at the particle surface however, the flow is chemically frozen elsewhere.

10
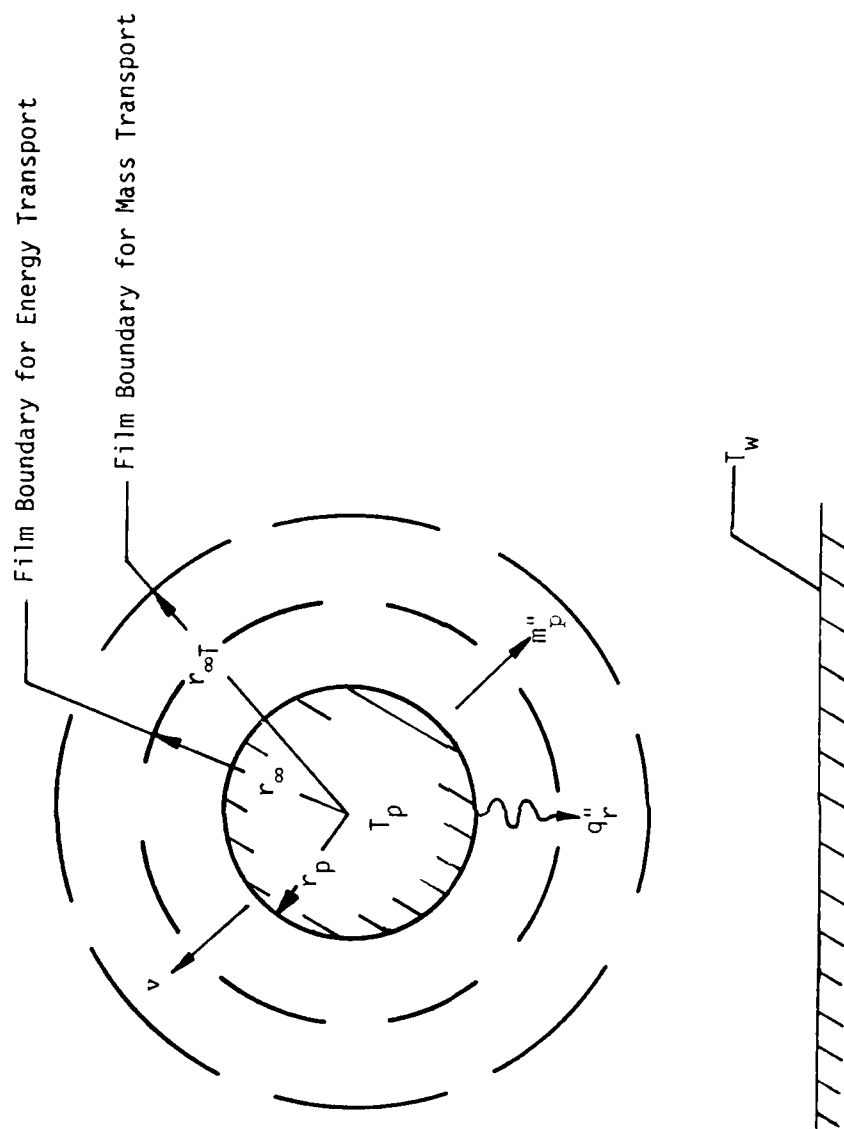
Figure 3. Sketch of the agglomerate reaction model.

11

These assumptions are generally similar to those employed in
recent analyses of carbon particle reaction [12,13].

3.2.1 Gas Phase Transport

The governing equations consist of equations for con-
servation of mass, energy and species. The latter equation can be
represented more conveniently in the present analysis, where equal
binary diffusivities are assumed, as equations for conservation of
elements--since elements are conserved during chemical reactions.
Employing the assumptions of the analysis, the following equations
apply [14].

$$\rho v r^2 = m_p'' \, r_p^{\,2} \qquad (1)$$

$$m_p'' \, r_p^{\,2} \frac{dh}{dr} = \frac{\lambda}{C_p} \frac{d}{dr} (r^2 \frac{dh}{dr}) \qquad (2)$$

$$m_p'' \, r_p^{\,2} \frac{d\tilde{Y}_i}{dr} = \rho D \frac{d}{dr}(r^2 \frac{d}{dr}(\tilde{Y}_i)), \quad i = 1,4 \qquad (3)$$

Four element fractions are considered in the analysis, $\tilde{Y}_{O_2}$, $\tilde{Y}_C$, $\tilde{Y}_{N_2}$ and $\tilde{Y}_{H_2}$.
Seven species were considered: O_2, N_2, CO_2, CO, H_2O, H_2 and OH. Following
Refs. 12 and 13, O was ignored on the grounds that its concentration is too
small, for temperatures below 4000K, for it to contribute significantly
to the reaction of carbon. Species and element concentrations are related
by the following mass balances

$$\tilde{Y}_i = \sum_{j=1}^{7} \nu_{ij} Y_j \quad , \quad i = 1,4 \qquad (4)$$

where ν_{ij} is the mass fraction of the ith element in the jth species.

12

The enthalpy appearing in Eq. (2) is given by

$$h = \sum_{i=1}^{7} Y_i h_i \tag{5}$$

where

$$h_i = C_{p_i} (T-T_{ref}) + h_{f_{i_{ref}}}^o \tag{6}$$

The boundary conditions for Eqs. (2) and (3) are as follows:

$$r=r_p, \quad h=h_p, \quad \tilde{Y}_i = \tilde{Y}_{i_p} \quad ; \quad r=r_\infty, \quad \tilde{Y}_i = \tilde{Y}_{i_\infty} \quad ; \quad r=r_{\infty_T}, \quad h=h_\infty \tag{7}$$

The ambient conditions are specified. The conditions at the particle surface must be determined from the analysis of surface reaction. This will be discussed later.

The general case is treated in Eq. (7), where the film radii for mass and heat transfer, r_∞ and r_{∞_T}, are not the same. These radii are found employing the usual correlations from film theory [11]. For mass transfer,

$$r_\infty/r_p = Sh/(Sh-2) \tag{8}$$

while for heat transfer

$$r_{\infty_T}/r_p = Nu/(Nu-2) \tag{9}$$

The Sherwood and Nusselt number correlations employed in Eqs. (8) and (9) are found from the following correlation [11].

$$(Nu \text{ or } Sh)-2 = \frac{0.555 \, Re^{1/2}(Pr \text{ or } Sc)^{1/3}}{(1+1.232/(Re(Pr \text{ or } Sc)^{4/3}))^{1/2}} \tag{10}$$

Equations (2) and (3) can be integrated, subject to the boundary conditions of Eq. (4), to yield

$$\tilde{Y}_i = \frac{(\tilde{Y}_{i\infty}-\tilde{Y}_{ip})\ \exp(-K/\xi) + Y_{ip}\ \exp(-K/\delta) - \tilde{Y}_{i\infty}\ \exp(-K)}{\exp(-K/\delta)-\exp(-K)} \qquad (11)$$

$$h = \frac{(h_\infty-h_p)\ \exp(-K/\xi Le) + h_p\ \exp(-K/\gamma Le) - h_\infty \exp(-K/Le)}{\exp(-K/\gamma Le)\ -\exp(-K/Le)} \qquad (12)$$

where

$$\xi = r/r_p \qquad (13)$$

$$\delta = r_\infty/r_p \qquad (14)$$

$$\gamma = r_{\infty_T}/r_p \qquad (15)$$

and K is a nondimensional particle mass loss parameter, defined as

$$K = m_p''\ r_p/\rho D \qquad (16)$$

A relationship between K and the Y_{ip} can be developed by noting that there is no net mass flux of the elements oxygen, hydrogen or nitrogen at the particle surface. Furthermore, the net mass flux of carbon at the surface is equal to m_p'', since the particle is assumed to be pure carbon. Therefore, at $\xi=1$, we have

$$\frac{d\tilde{Y}_i}{d\xi} = K\tilde{Y}_i \qquad i = 1,4\ ;\ \ i \neq C \qquad (17)$$

14

$$\frac{d\overset{\scriptscriptstyle\vee}{Y}_C}{d\xi} = -K(1-\overset{\scriptscriptstyle\vee}{Y}_C) \tag{18}$$

Taking the derivative of Eq. (11) and substituting into Eqs. (17) and (18) yields the following

$$\overset{\scriptscriptstyle\vee}{Y}_{i_p} = \overset{\scriptscriptstyle\vee}{Y}_{i_\infty} \exp(K(\delta^{-1}-1)) \quad , \quad i = 1,4 \quad , \quad i \neq C \tag{19}$$

$$\overset{\scriptscriptstyle\vee}{Y}_{C_p} = 1-(1-\overset{\scriptscriptstyle\vee}{Y}_{C_\infty}) \exp(K(\delta^{-1}-1)) \tag{20}$$

Employing the usual sign convention that convection to the surface of the particle is positive, and recalling that equilibrium has been neglected in the gas phase, yields

$$q_c'' = -\lambda\frac{dT}{dr}\Big)_{r_p} = \frac{-\lambda}{C_p} \frac{dh}{dr}\Big)_{r_p} \tag{21}$$

where the second part of Eq. (21) follows from the assumption of constant gas phase specific heat. Taking the derivative of Eq. (12) and evaluating the resulting expression at $r = r_p$, yields

$$\frac{q_c'' C_p}{K(h_\infty - h_p)} = \frac{-\exp(-K/Le)}{\exp(-K/\gamma Le) - \exp(-K/Le)} \tag{22}$$

Given K, Eqs. (19) and (20) yield the four element mass fractions at the surface of the particle. Equation (11) then provides four of the equations to determine the seven unknown species mass fractions. Imposing the condition of chemical equilibrium, yields the three more equations needed to determine the Y_i. The following dissociation reactions were employed

$$H_2O \; \overset{K_{Y_1}}{\rightleftharpoons} \; H_2 + 1/2 \; O_2$$

$$H_2O \; \overset{K_{Y_2}}{\rightleftharpoons} \; 1/2 \; H_2 + OH \tag{23}$$

$$CO_2 \; \overset{K_{Y_3}}{\rightleftharpoons} \; CO + 1/2 \; O_2$$
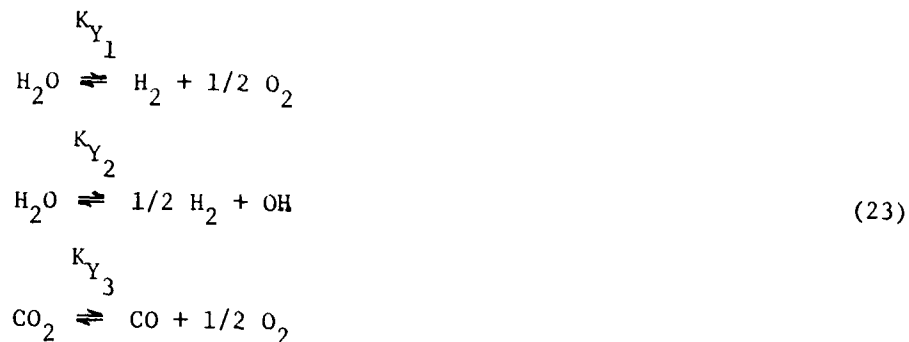
This yields the following equilibrium requirements

$$K_{Y1} \; p^{-1/2} = Y_{H_2} \; Y_{O_2}^{1/2}/Y_{H_2O} \tag{24}$$

$$K_{Y2} \; p^{-1/2} = Y_{H_2}^{1/2} \; Y_{OH}/Y_{H_2O} \tag{25}$$

$$K_{Y3} \; p^{-1/2} = Y_{CO} \; Y_{O_2}^{1/2}/Y_{CO_2} \tag{26}$$

Since the K_{Y_i} are known functions of temperature, Eqs. (4), (19),
(20) and (24)-(26), allow $\tilde{Y}_{i_p}$ and Y_{i_p} to be determined, given the
ambient composition, K, and the surface temperature. The next section
will consider the relationship between K and the Y_{i_p}.

Constant average properties were employed at each instant of time,
using methods similar to earlier work in this laboratory [9]. The
methods used to compute properties are described in Appendix A.

3.2.2 Surface Reactions

The reaction of carbon is a complex process, particularly
when the material is in a combustion product mixture containing many
species. Reaction mechanisms of carbon involving O_2, CO_2, H_2O, H_2, OH
and O can play a role [15,16]. During the present analysis, only the
first three species O_2, CO_2 and H_2O were considered. The present
methodology, however, is applicable to more complex treatment of
reaction as new information becomes available.

16

Other problems that must be considered, include: 1) reaction is not just limited to the apparent outer surface, since pores are present; and 2) the presence of a catalyst influences reaction rates. The effect of both these factors was treated in the present analysis by introducing empirical area/reactivity multiplication factors for each reaction contributing to the consumption of carbon. The values of the area/reactivity factors were specified by matching predictions and measurements.

The reaction rates for carbon with oxygen and carbon dioxide employed the same kinetic parameters as Libby and Blake [13]. The reactions are assumed to proceed by the following global expressions

$$C + 1/2 \ O_2 \ \xrightarrow{R_1} \ CO \qquad\qquad (27)$$

$$C + CO_2 \ \xrightarrow{R_2} \ 2CO \qquad\qquad (28)$$

where the specific rate constants are

$$R_1 = K_1 \ P_{O_2} \quad , \quad R_2 = K_2 \ P_{CO_2} \qquad\qquad (29)$$

where

$$K_i = A_i \ \exp(-E_i/RT) \quad , \quad P_i = pMY_i/M_i \qquad\qquad (30)$$

The specific values of the chemical parameters appearing in Eqs. (29) and (30) are summarized in Table 3.

The reaction rate expression for water vapor employs the results of Johnstone, et al. [17]. The reaction mechanism is as follows [15]

17

Table 3

Summary of Reaction Rate Parameters

i	A	$E(kcal/gmol)$
1	87100 kg/m^2s atm	35.8
2	2470 kg/m^2s atm	41.9
3	5.15×10^{-3} kg/m^2s atm[a]	32.7
4	9.42×10^{-11}	-60.8
5	7.07×10^{-16}	-79.3

Slurry	Reactivity Factor, a_i[b]
noncatalyzed	58.2
catalyzed	70.6

[a]Assuming a surface area of reaction of 1.15 m^2/g of carbon, which is the average surface area over the period of reaction [17].

[b]Reactivity factor taken to be the same for reaction with O_2, CO_2 and H_2O.

$$C + H_2O \rightleftharpoons H_2 + C(O) \tag{31}$$

$$C(O) \rightarrow CO \tag{32}$$
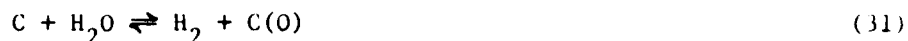
The reaction rate of carbon due to the presence of water vapor can then be expressed as

$$R_3 = \frac{K_3 P_{H_2O}}{1 + K_4 P_{H_2} + K_5 P_{H_2O}} \tag{33}$$

The parameters in this case, appearing in Table 3, were obtained from Ref. 17. In order to obtain the rate constants of Table 3 for these reactions, it was necessary to estimate the actual surface area for reaction for the experiments of Ref. 17. The surface areas are taken as the average over the range of reaction, measured by nitrogen adsorption [17].

The total reaction of carbon was obtained as the sum of the rates or O_2, CO_2 and H_2O, ignoring potential interactions between the reactants. This yields

$$K = \frac{r_p}{\ .D} \sum_{i=i}^{3} \alpha_i R_i \tag{34}$$

where the α_i appearing in Eqs. (34) are the area/reactivity multiplication factors. These parameters were varied in the present investigation in order to match burning rate results to predictions. In general the presence of pores and a catalyst result in α_i values greater than unity.

3.2.3 Agglomerate Life-History Computations

Given the temperature and size of the particle, and the ambient conditions, solution of Eqs. (4)-(31) are sufficient to provide Y_{i_p}, Y_{i_p}, q_c'' and K. The variation of the size and temperature of the particle are determined by solving equations for conservation of particle mass and energy.

Conservation of mass for the particle is

$$\frac{d}{dt}\left(\frac{4}{3}\pi r_p^3 \rho_s\right) = - 4\pi r_p^2 m_p''$$ (35)

Assuming that the particle density is constant,

$$\frac{dr_p}{dt} = - \rho DK/\rho_s \, r_p$$ (36)

introducing K from Eq. (16).

Conservation of energy at the surface of the particle yields

$$\frac{d}{dt}\left(\frac{4}{3}\pi r_p^3 \rho_s h_s\right) = 4\pi r_p^2 \, (\Sigma m_i'' h_i + q_c'' + q_r'')$$ (37)

where

$$q_r'' = \sigma \, \varepsilon \, (T_p^4 - T_w^4)$$ (38)

and T_w is the temperature of the enclosure surrounding the hot gas. Simplifying Eq. (34) by introducing conservation of mass, Eq. (17), yields

$$\frac{dT_p}{dt} = \frac{-3}{(\rho_s C_s r_p)} \, [m_p'' \, (h_{cp} - h_s) + q_c'' + q_r'']$$ (39)

During some experimental conditions, the rate of radius change of the particle was relatively slow. In this case, the particle would reach a quasisteady equilibrium condition where its rate of temperature

20

change with time was small. These quasisteady particle temperatures were determined by setting the left-hand side of Eq. (39) equal to zero and solving the equation for particle temperature.

Conservation of particle momentum would yield an additional equation to determine the motion of the particle. Since supported particles were considered during this investigation, these results are not needed and will not be considered here.

The initial conditions for Eqs. (36) and (39) are

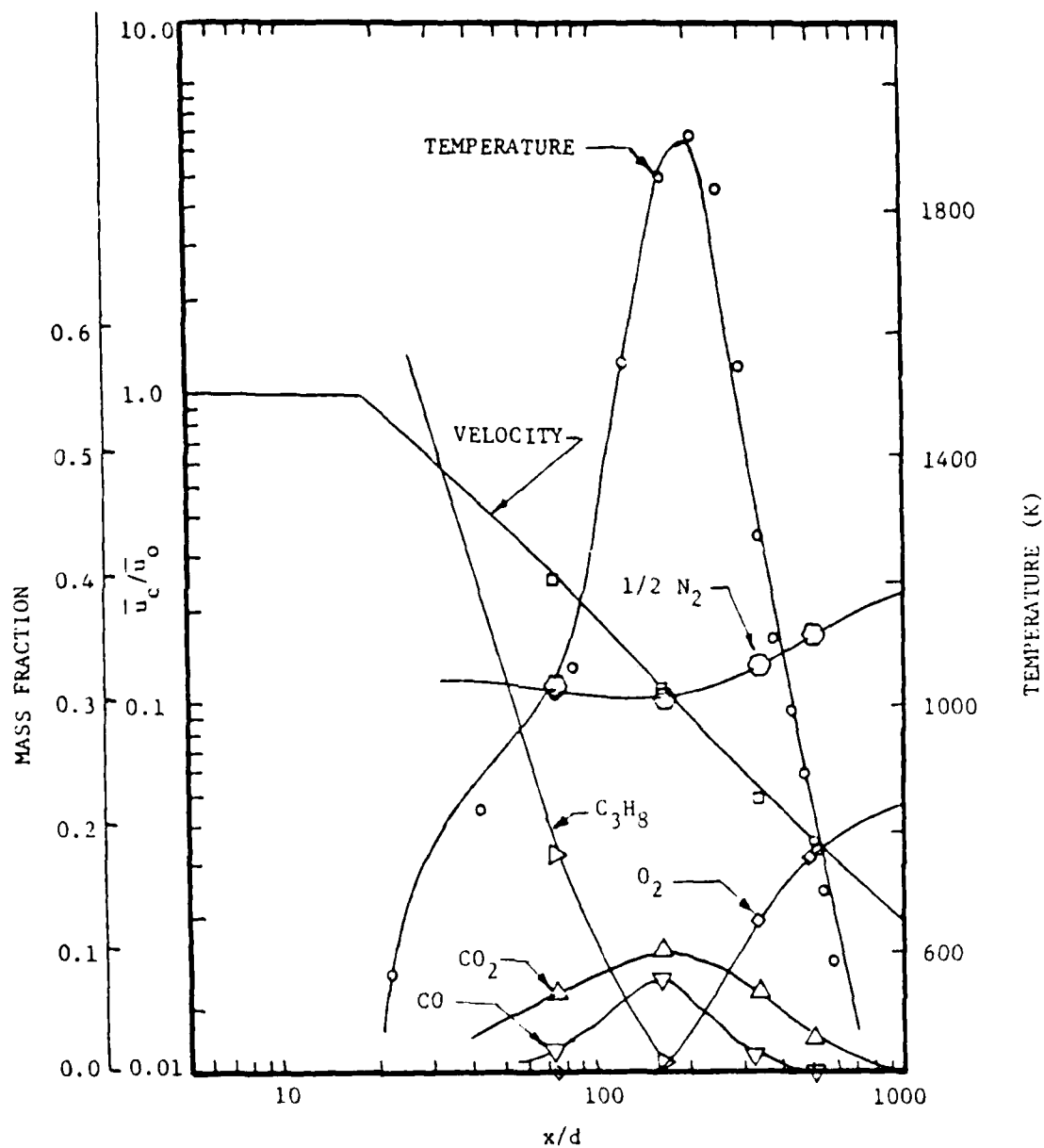$$t = 0, \quad r_p = r_{p_o}, \quad T_p = T_{p_o} \tag{40}$$

Equations (36) and (40) were numerically integrated on the computer, using Gear's method. The nonlinear system of algebraic equations which must be satisfied in order to determine Y_{i_p}, Y_{i_p}, q_c'', etc., were solved using the Newton-Raphson method, given the current values of T_p and r_p, and the ambient conditions, at each instant of time. Quasisteady burning rates were determined by iterating on T_p, until the left-hand side of Eq. (39) was zero.

4. Results and Discussion

   4.1 General Observations

   Figure 4 is an illustration of the variation of mean properties along the centerline of the propane flame [9]. Near the injector exit, gas velocities and the concentration of propane are relatively high, while the temperature is low and oxygen is absent. Moving downstream, the gas velocity and the concentration of propane decrease monatonically. The temperature increases at first, reaching a maximum at the point where the fuel has disappeared and combustion product concentrations are highest. Beyond this location of the flame, the flow decays. In this region, temperatures and product gas concentrations decrease, while oxygen and nitrogen concentrations increase.

Similar to our previous slurry combustion study [4], present measurements were obtained along the centerline of this flame. Also marked on Fig. 4 are various combustion regions determined for both catalyzed and noncatalyzed slurry drops during our earlier work [4]. Combustion performance for each of these regimes described in Table 4.

21

10.0

TEMPERATURE

1800

0.6

1.0

VELOCITY

1400

MASS FRACTION

0.5

$\bar{u}_c/\bar{u}_o$

0.4

$1/2\ N_2$

TEMPERATURE (K)

0.3   0.1

0.2

C_3H_8

O_2

0.1

CO_2

600

CO

0.0   0.01

10   100   1000

x/d

noncatalyzed slurry   F   NC   FC | E

catalyzed slurry   F   NC   FC |G| E

Figure 4.   Flow properties and slurry drop combustion regions in
             the turbulent flame [4].

22

Table 4

Summary of Slurry Drop Combustion Regions in the Turbulent Flame

Region[a]	Designation	Description
Fragmentation	F	The liquid fuel evaporated without an envelope flame; however, a diffuse luminous wake was observed. When all the liquid was gone, some of the carbon agglomerate was fragmented into 3-5 large flakes. A carbon agglomerate also remained on the probe.
Noncombusting	NC	The liquid fuel evaporated without an envelope flame; however, a diffuse luminous wake was observed. When all the liquid had evaporated, a luminous wake or reduced intensity was still observed. A carbon agglomerate remained on the probe.
Full combustion	FC	An envelope flame was observed around the particle until the liquid fuel was consumed. After a dark period, the carbon agglomerate began to glow. Glowing continued until virtually all the carbon was consumed.
Glowing	G	The liquid fuel evaporated with no envelope flame observed. Some time after the liquid was gone (2-15 s for present test conditions), the carbon agglomerate began to glow. Glowing persisted until virtually all the carbon was consumed. This region was only observed for the catalyzed slurry.
Evaporation	E	The liquid fuel evaporated with no envelope flame observed. Glowing of the carbon agglomerate was not observed. No change of the particle size was observed once the liquid was gone for the noncatalyzed slurry. Some reaction of the catalyzed slurry was observed in the upstream end of this zone.

[a] In order of increasing distance from the injector.

23

The present measurements were confined to the range $225 \leq x/d \leq 510$. This includes the full combustion (FC), glowing (G) and evaporation (E) regions. In the first two regions, combustion of the carbon agglomerate is observed, although the second region is only observed for the catalyzed slurry. In the evaporation region, combustion of the agglomerate is quenched. This region is of marginal interest for the present study, however, it is desirable to predict its onset. Table 5 is a summary of flow properties at each of the drop test locations.

Figure 5 is an illustration of a noncatalyzed slurry drop-life-history at $x/d = 297.5$, where agglomerate reaction rates are reasonably high. Particle diameter and temperature are plotted as a function of time. The time scale has been expanded during the first portion of the plot, when the liquid is **gasified**, since this period is relatively short.

The four main stages of slurry drop combustion are quite apparent in Fig. 5. The initial phase of the process involves heat-up of the particle, approaching the wet-bulb temperature for liquid evaporation (which is somewhat below the boiling temperature of the liquid [11]). In this period, the rate of liquid evaporation is relatively low and the particle diameter remains nearly constant. As the surface temperature nears the wet-bulb temperature, the rate of gasification increases, beginning the second stage of the process. During the second stage, the particle diameter decreases while the particle temperature remains nearly constant. The third stage involves heat-up of the agglomerate, once all the liquid has evaporated. The variation of particle diameter is relatively slow in this period, due to low carbon reaction rates at low temperatures. As particle temperatures increase, reaction rates increase as well, signaling the onset of the fourth stage of the process. During the fourth stage, the agglomerate reacts, with particle temperatures near the gas temperature. In this regime, the particle temperature can be either above or below the gas temperature, depending upon the magnitudes of energy released by reaction and heat transport by convection and radiation. These quantities tend to vary with particle size, so there is no fixed particle temperature in the fourth regime, even though ambient conditions are fixed. As the particle becomes small, however, convection heat transfer dominates, and the particle tends to approach the local gas temperature.

It is evident from the results illustrated in Fig. 5, that heat-up and reaction of the agglomerate comprises the bulk of the lifetime of the particle.

4.2 Agglomerate Burning Rates

Figure 6 is an illustration of predicted and measured agglomerate burning rates for noncatalyzed drops. Results are shown for various positions in the range $297 \leq x/d \leq 510$. This region is in the lean portion of the propane flame, corresponding to an equivalence ratio range of 0.761-0.272. For these conditions, reaction of carbon with oxygen dominates the process, and the effects of CO_2 and H_2O are small.

24

Table 5

Summary of Flame Properties at Droplet Test Locations

| $\frac{x}{d}$	T (K)	u (m/s)	ϕ	Mass Fractions				
				O_2	CO_2	CO	N_2	H_2O
170	1841	9.93	1.350	0.006	0.101	0.079	0.653	0.161
212.5	1903	8.14	0.939	0.021	0.094	0.051	0.689	0.145
255	1824	6.15	0.870	0.076	0.079	0.039	0.677	0.129
297.5	1541	4.82	0.761	0.093	0.075	0.031	0.688	0.113
340	1271	4.35	0.557	0.122	0.066	0.016	0.699	0.097
382.5	1101	4.21	0.484	0.136	0.057	0.013	0.705	0.0895
467.5	887	3.90	0.348	0.163	0.038	0.007	0.717	0.075
510	779	2.93	0.272	0.176	0.029	0.004	0.724	0.067
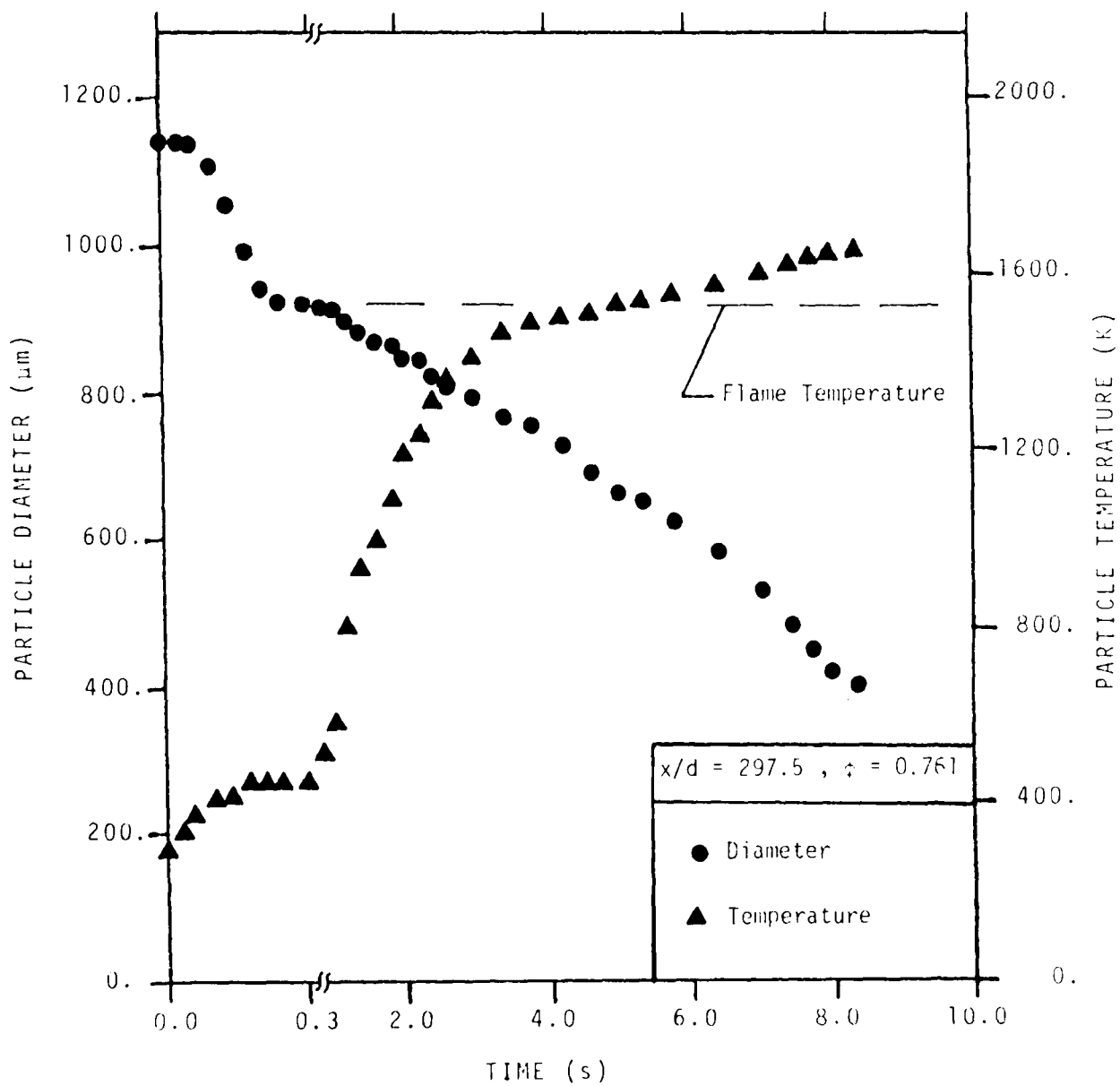
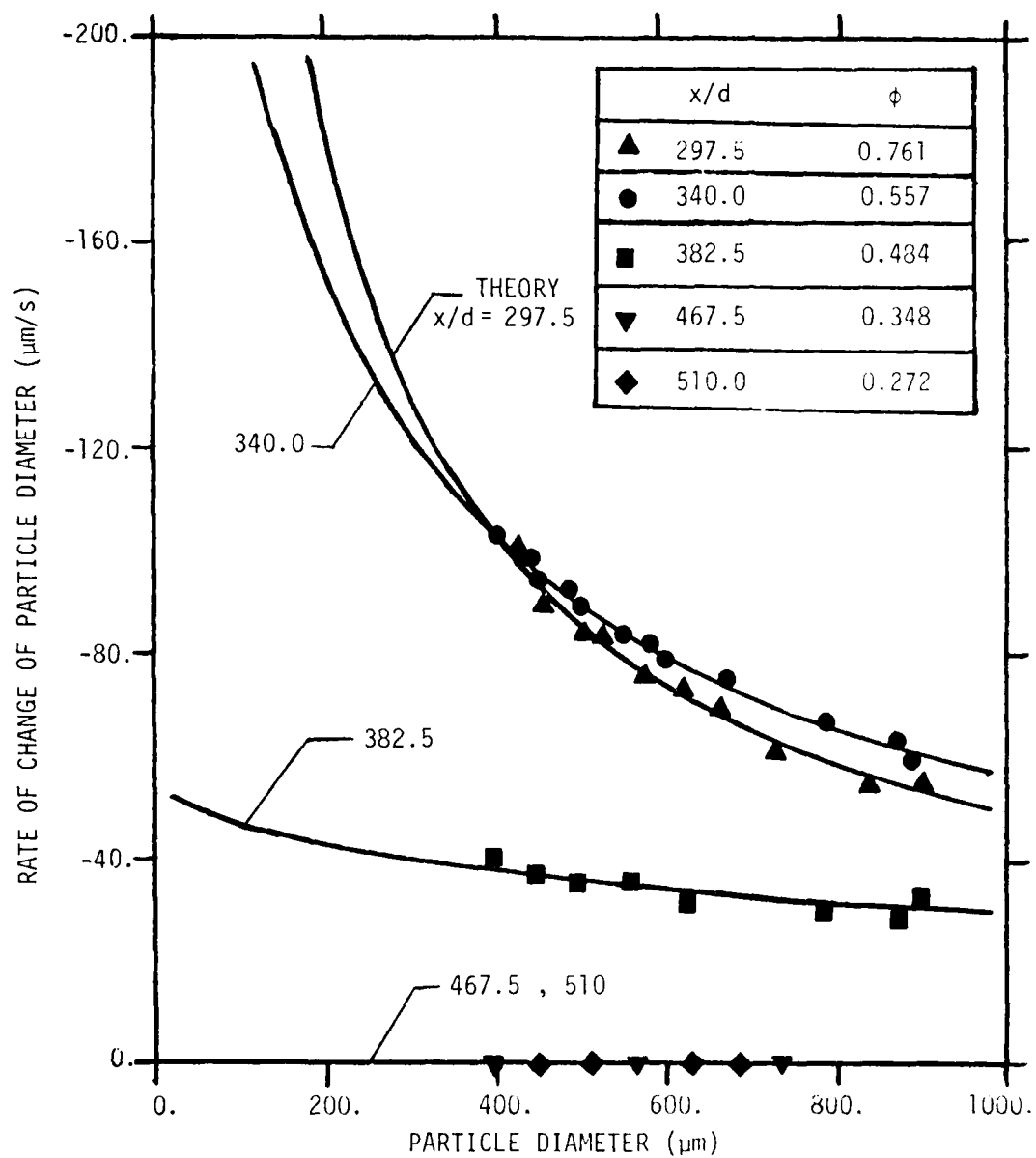Figure 5. Slurry drop life-history at x/d = 297.5.

Figure 6. Quasisteady reaction rates for a noncatlyzed agglomerate.

27

In Fig. 6, predictions have been matched to the measurements at
x/d = 382.5, by selecting a reactivity factor of a_i = 58.2 for all
the reactions. This parameter was then held constant for the re-
maining computations, a procedure which yields a reasonably good
correlation of the remaining measurements, including both
effects of particle size (in the range 400-730 μm) and position in
the flame. The low reaction rates indicative of the evaporation
region were also predicted reasonably well. Thus the model demon-
strates some potential for predicting quenching of agglomerate
reaction.

There are two main combustion limits for carbon agglomerates.
The first limit involves reaction rate control, where reaction rates
are relatively low in comparison to diffusion rates, and the concen-
trations of gaseous reactants at the surface of the particle are
nearly the same as in the surroundings. This regime is characterized
by the burning rate being relatively independent of particle diameter,
e.g., results for x/d ≥ 382.5 in Fig. 6 approach the reaction rate
limit.

The second limit involves diffusion control, where reaction rates
are high in comparison to diffusion rates, and the concentrations of
reactant gases at the surface of the particle are small. The variation
of the burning rate is influenced by particle diameter in this region,
showing a dependence

$$- \frac{dr_p}{dt} \sim 1/r_p^{(0.5 \text{ to } 1.0)} \tag{41}$$

The power of r_p, in Eq. (41), tends to increase as the Reynolds number
of the particle decreases. From this argument, it is apparent that
the higher reaction rates illustrated in Fig. 6 (x/d = 297.5, 340.0) are
approaching the diffusion controlled limit. Diffusion rates become
large for small particles; therefore, all regions of the flow would
eventually exhibit kinetic control for sufficiently small particles.

Figure 7 is an illustration of predicted and measured burning rates
for a catalyzed agglomerate. These test results were limited to
x/d = 297.5, 340.0 and 382.5. Reaction of the agglomerate is nearly
diffusion controlled at the first two positions. Therefore, burning
rates with and without catalyst are essentially the same at these
locations. At x/d = 382.5, however, the burning rate is more nearly
reaction rate controlled. At this position, the use of the catalyst
results in a 20-25 percent increase in the burning rate. Naturally,
the effect of the catalyst is even larger at positions farther down-
stream, e.g., adding catalyst reduces the lean limit for quenching from
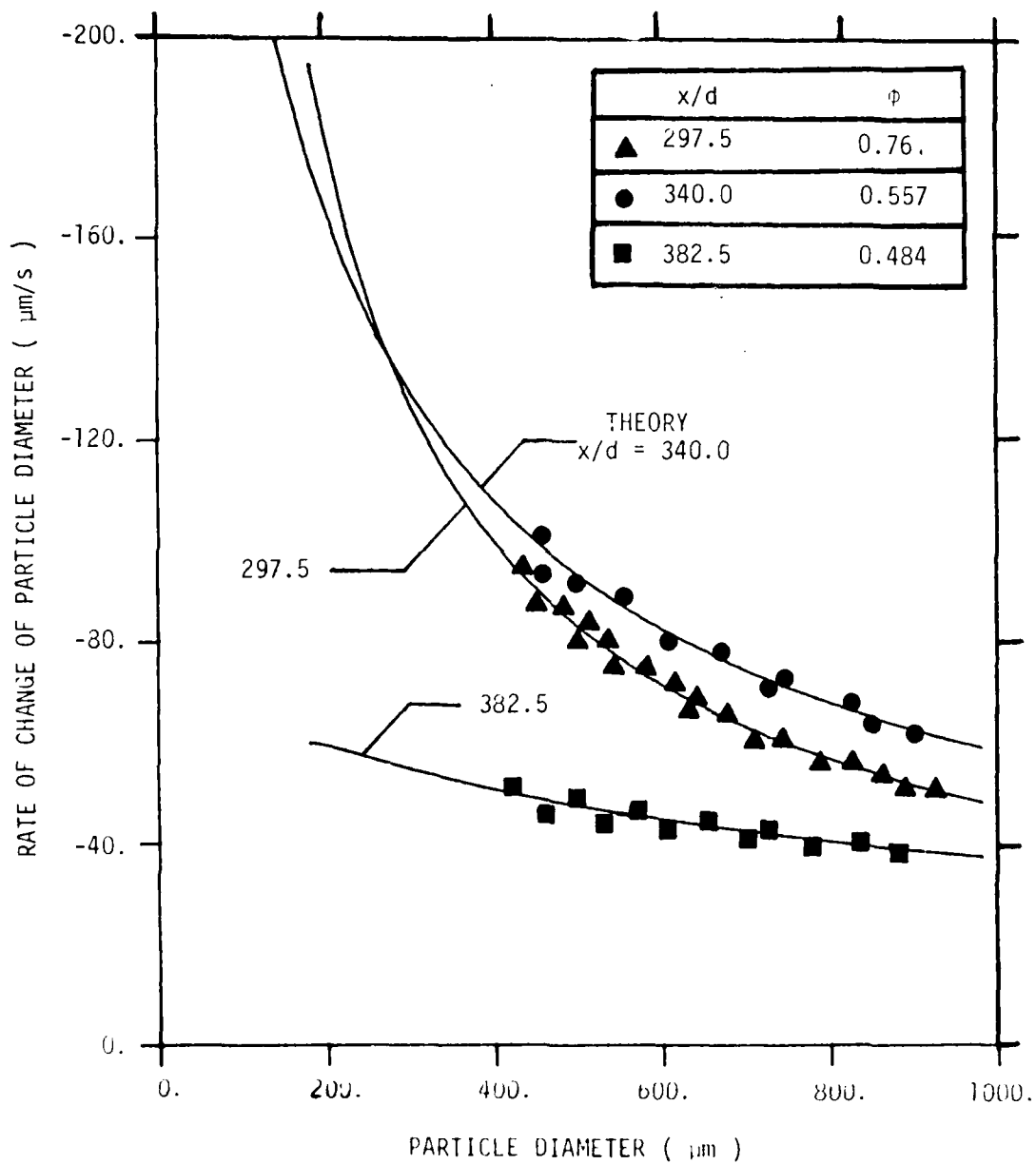0.37 to 0.21 [4].

Figure 7. Quasisteady reaction rates for catalyzed agglomerates.

The presence of catalyst is treated in the theory by adjusting the area/reactivity factor. Selecting a_i = 70.6, for all the reactions, yields the theoretical results illustrated in Fig. 7. With this choice, the predictions are in reasonably good agreement with the measurements.

Another property of catalyzed slurries was their tendency to spontaneously shatter from time to time. This shattering occurred after all the liquid had apparently evaporated. This behavior could be influenced by the presence of the thermocouple support, and was not consistently observed. If shattering does persist for small unsupported particles, this would provide another (physical) mechanism for the improved combustion properties observed for catalyzed slurries [3]. Tests with unsupported particles having sizes more typical of sprays will be required to resolve this question.

4.3 Agglomerate-Life-Histories

Agglomerate-life-histories were computed at x/d = 255-510, for noncatalyzed slurries. The resulting comparison between predicted and measured particle diameters and temperatures as a function of time are illustrated in Figs. 8-13. For reference purposes, the local temperature of the flow is also shown on each plot.

The initial condition for the computations illustrated in Figs. 8-13, was the temperature and diameter of the agglomerate, when all the liquid had evaporated. The comparison between predictions and measurements is seen to be quite good. This is partly expected, since the model was capable of correlating the burning rate measurements for this range of flame conditions. However, the results show that the model gives a good representation of the heat-up of the particle as well, where reaction effects are small, for various particle sizes and ambient temperatures, compositions and velocities, c.f. Table 5. At higher temperature levels, heat-up is also influenced by reaction and radiation to the surroundings. It is promising that the model appears to be capable of treating these effects as well.

The range of conditions illustrated in Figs. 8-13 is such that particle heat-up is terminated at temperatures both above and below the local gas temperature. This behavior is due to the opposing effects of reaction, tending to increase particle temperatures above the gas temperature, and radiation, which tends to reduce the particle temperatures below the gas temperature. In all cases, however, convection would dominate the process as the particle becomes small and the particle would finally tend to approach the gas temperature. This is not observed in Figs. 8-13 due to the finite-sized thermocouple bead used to mount the slurry drop.

4.4 Limitations of the Study

While the model shows an encouraging capability to predict the combustion properties of carbon agglomerates, several limitations of the present evaluation should be recognized. The main limitation
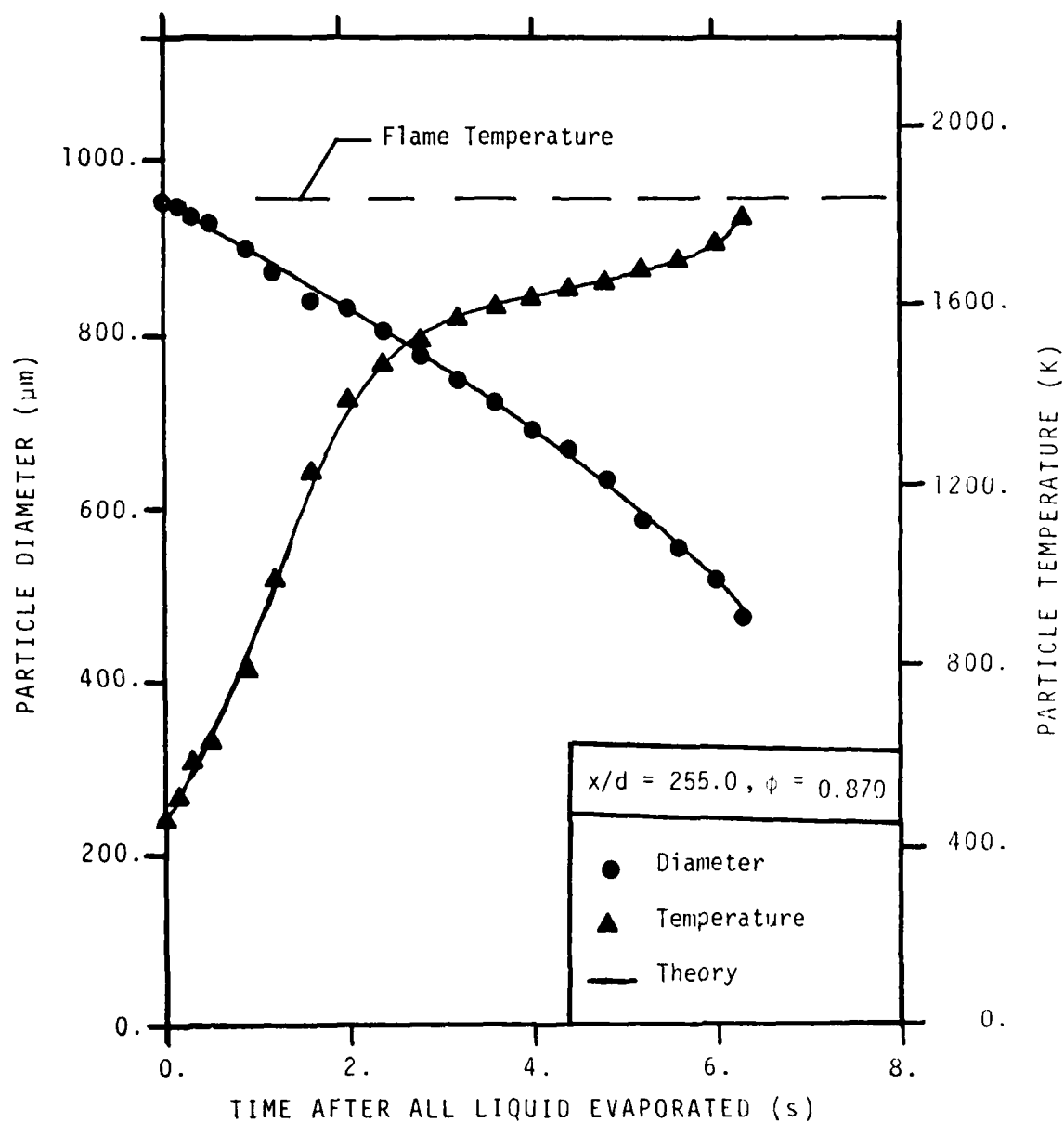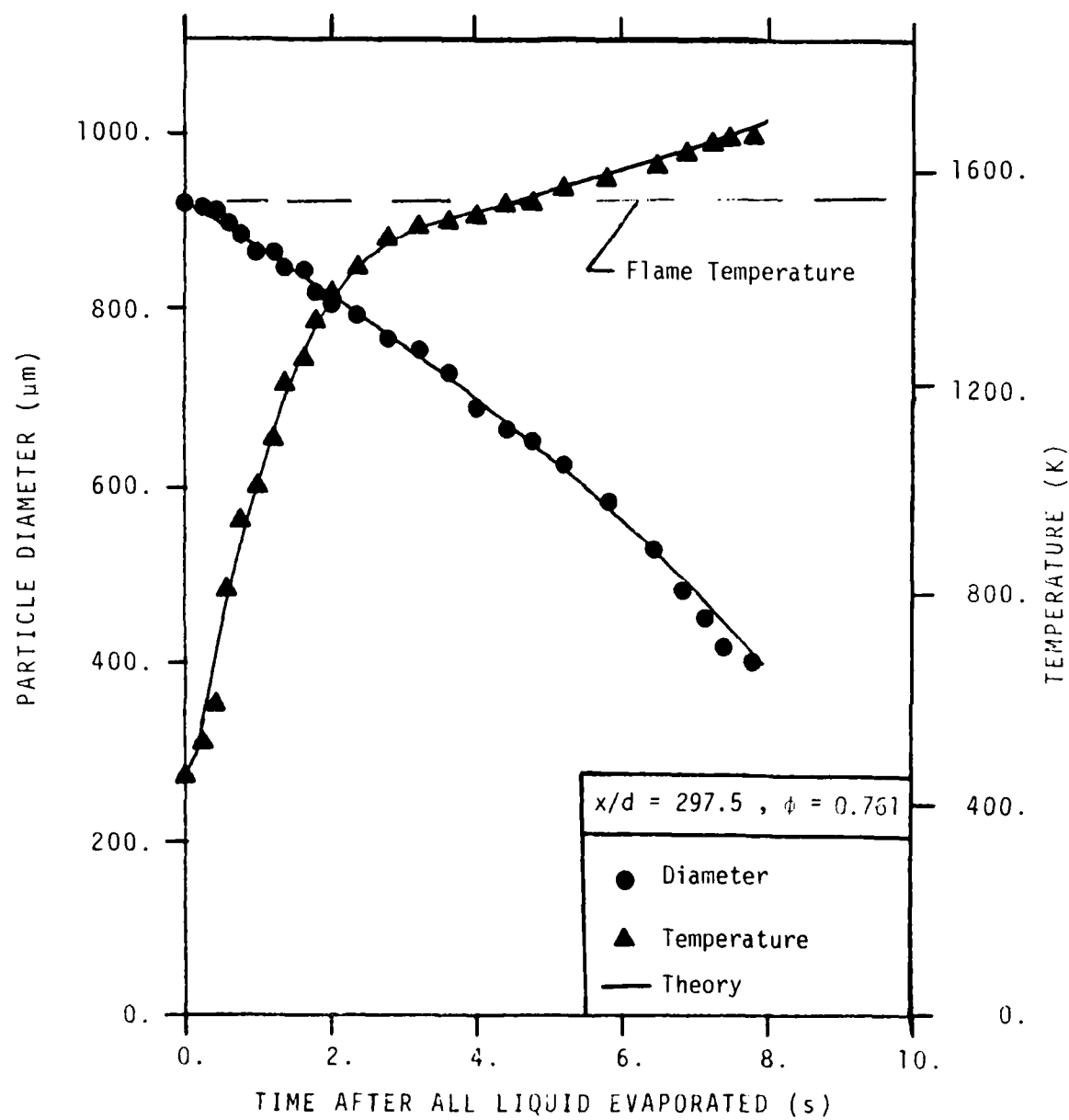
Figure 8. Agglomerate-life-history at x/d =255.0.
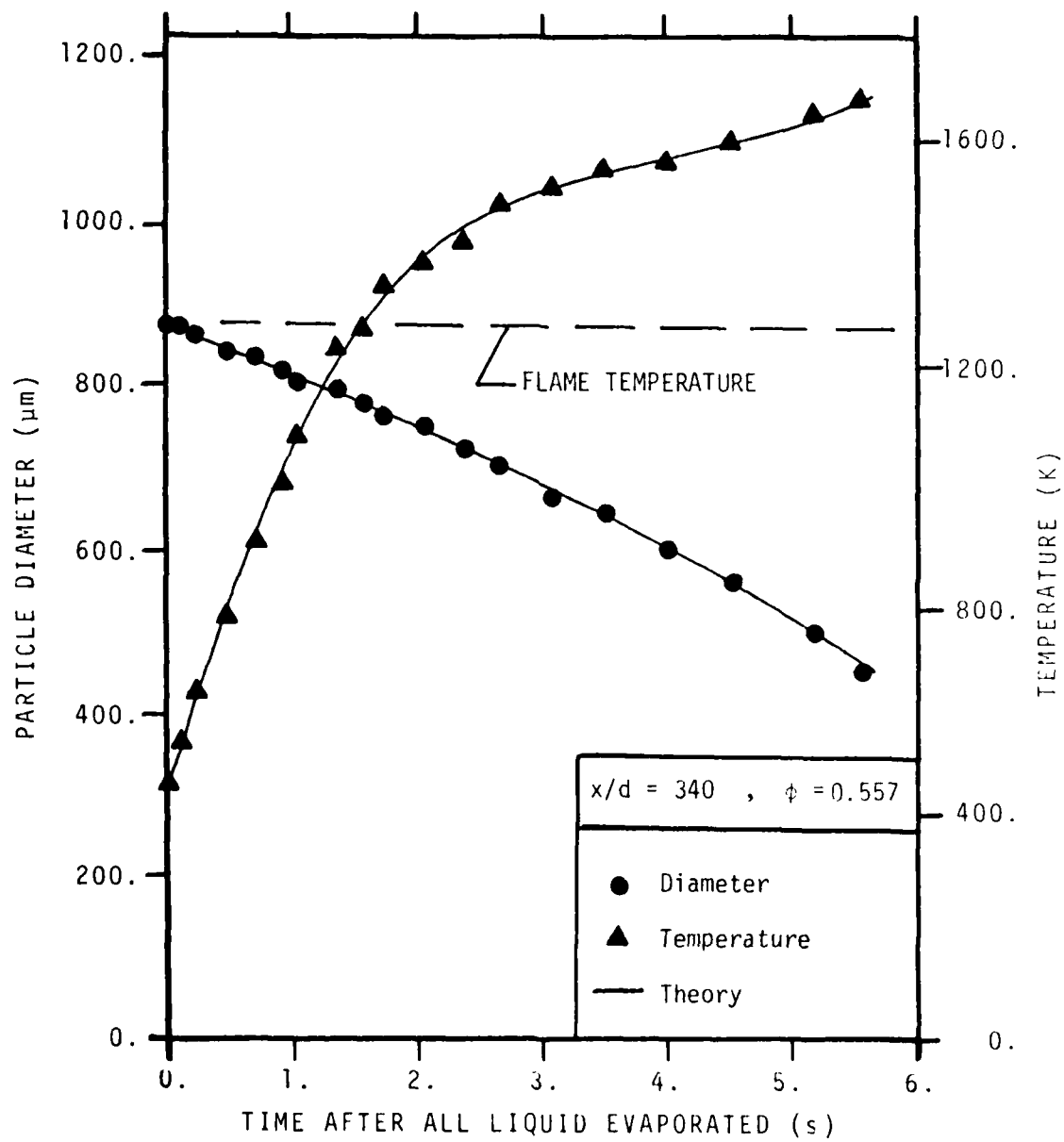
Figure 9.   Agglomerate-life-history at x/d = 297.5.
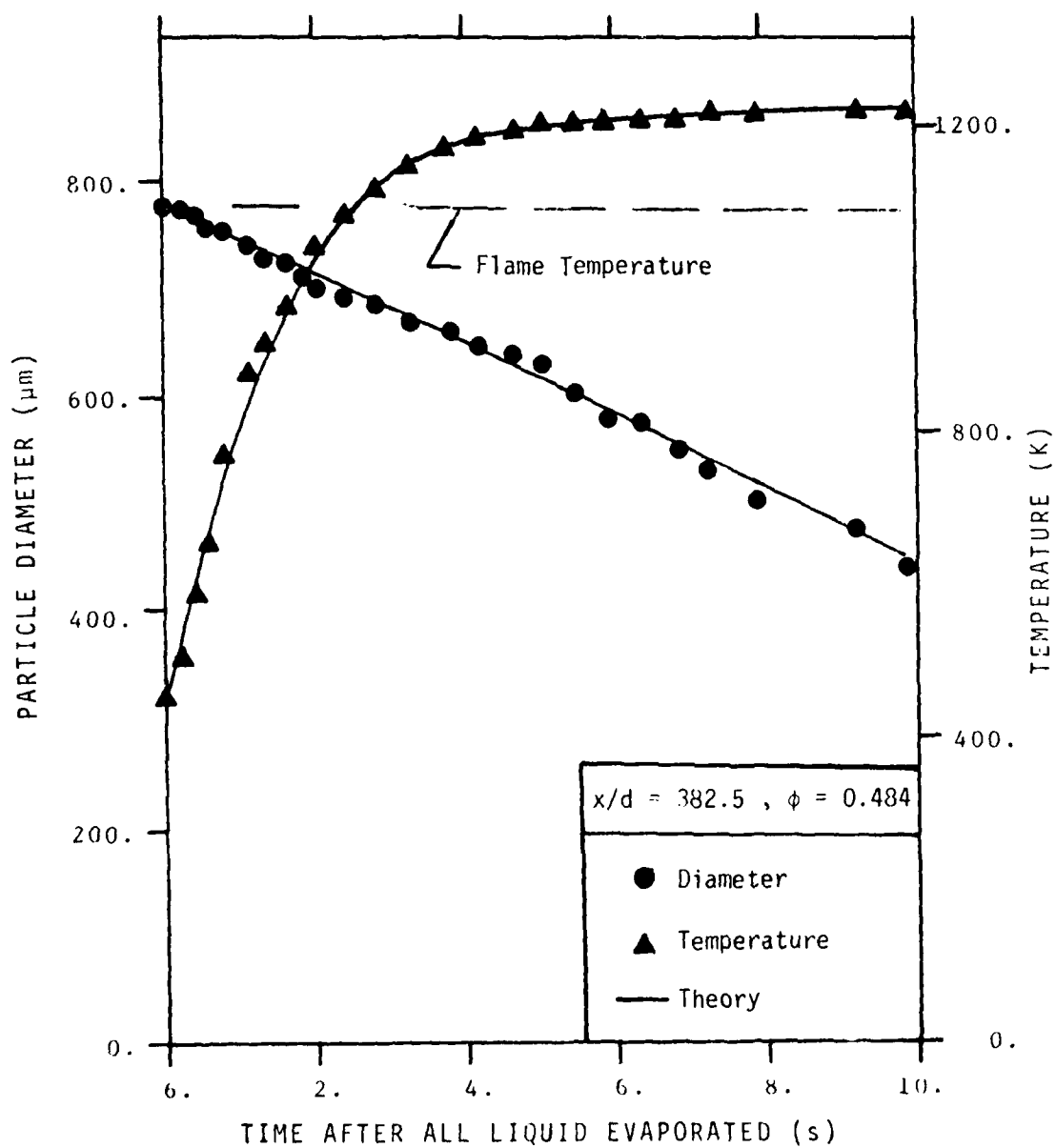
32

Figure 10. Agglomerate-life-history at x/d = 340.0.
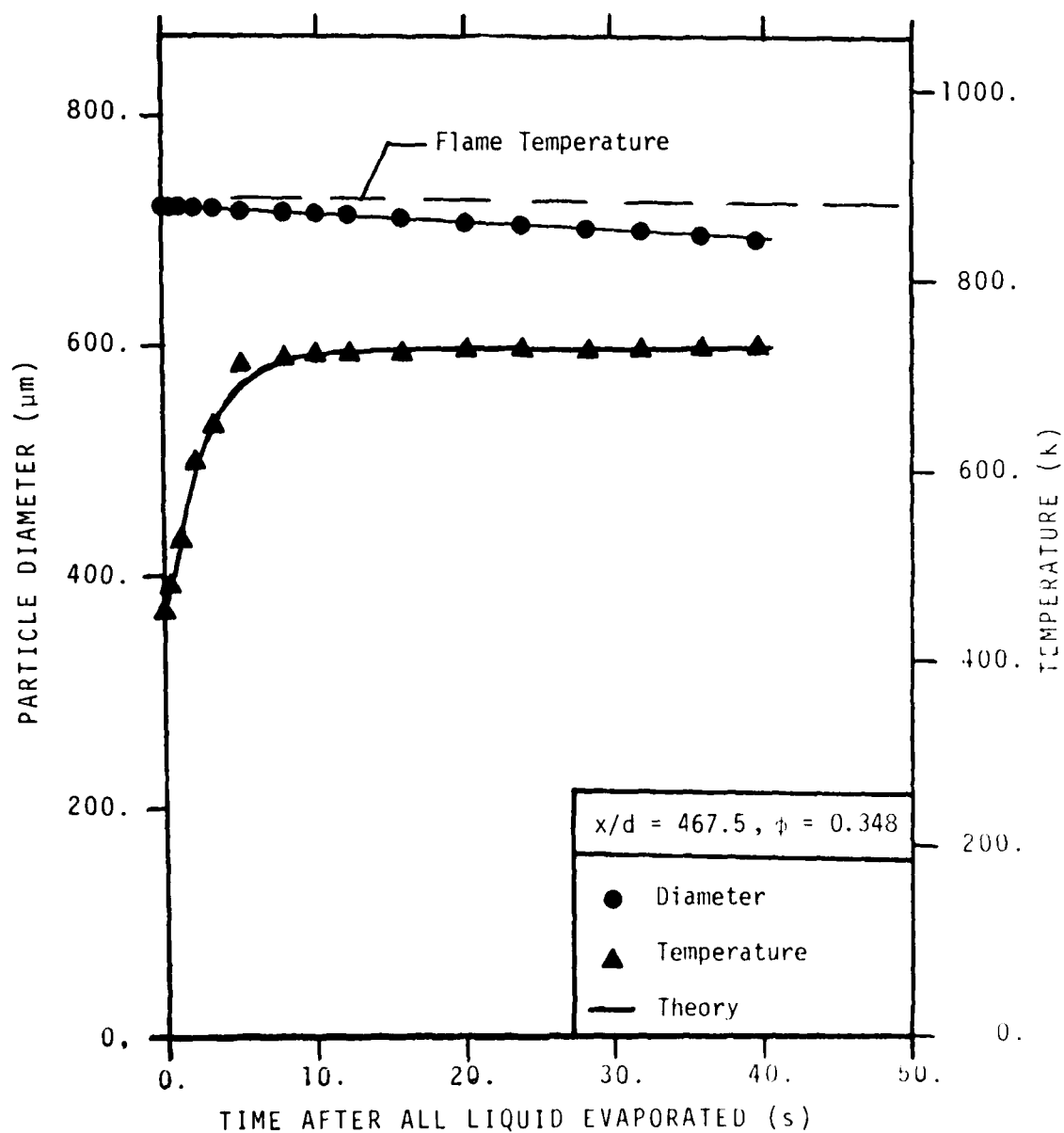
Figure 11. Agglomerate-life-history at x/d = 382.5.
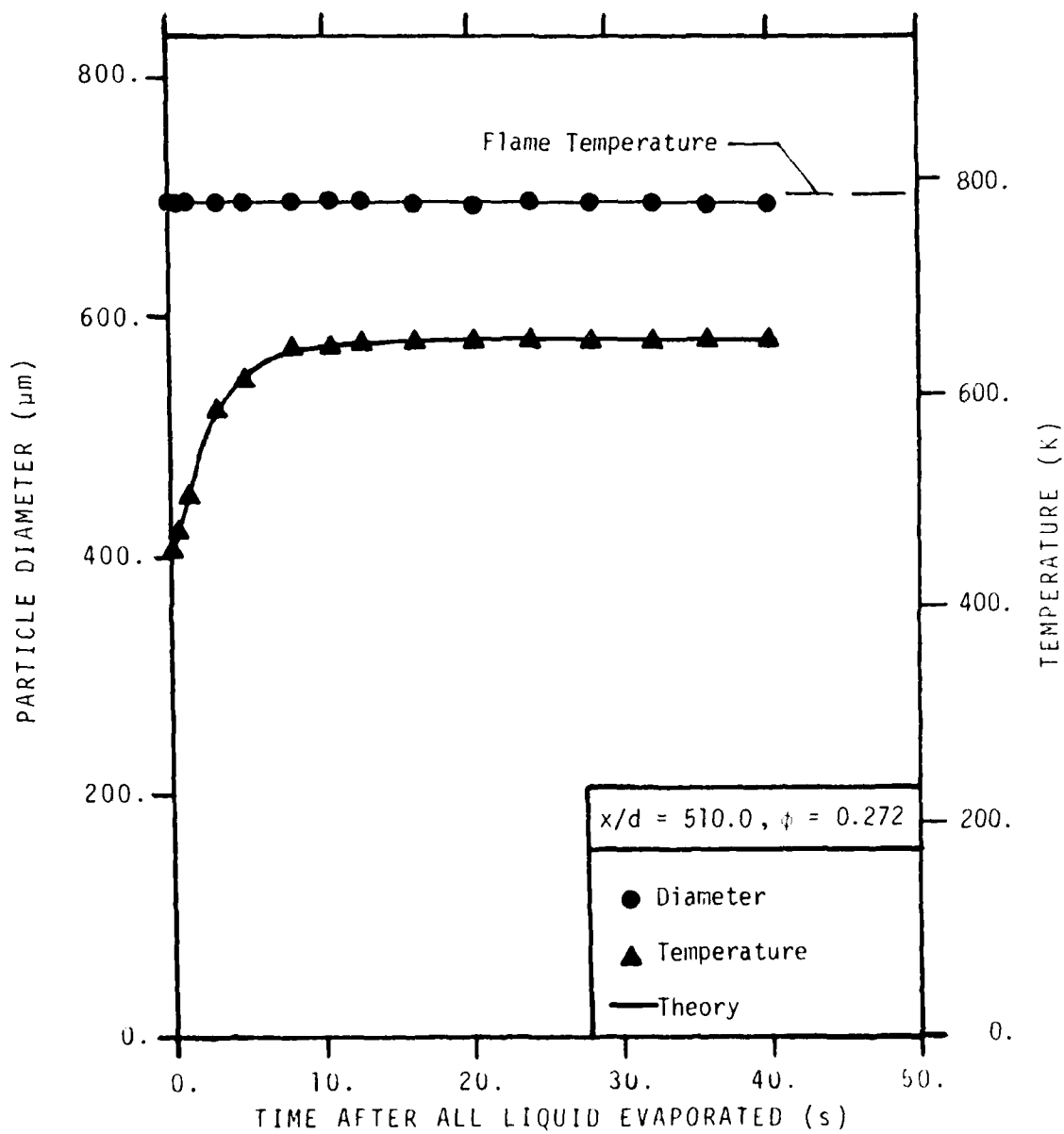
Figure 12.   Agglomerate-life-history at x/d = 467.5.

Figure 13. Agglomerate-life-history at x/d = 510.0.

of this study is the large particle sizes examined,
400-1000 µm, in comparison to the sizes expected in
practical combustors. The major difficulty involves the present
specification of area/reactivity multiplication factors—which were
taken to be constant during the present study. For large particles,
diffusion of reactant gases is not expected to penetrate very far
into the particle, while very small particles would have reactant
gases penetrated throughout their volume. Therefore, the relative
proportions of apparent surface to actual reaction areas will tend
to increase as particle sizes become small. Therefore, it is ex-
pected that the area/reactivity multiplication factor would tend to
increase as particle sizes are reduced. The magnitude of this change
can only be established by additional study. Naturally, this effect
would only be important outside the diffusion controlled limit.

Present test conditions were not sufficiently varied to establish
the appropriate area/reactivity multiplication factors for the carbon
dioxide and water vapor reactions, since oxygen dominated carbon
reaction when the basic reaction parameters of Table 5 are used in the
analysis. It is unlikely that the effect of pores, surface properties
or catalyst would act the same for each reactant. Therefore, use of
the present findings should be limited to conditions where reaction of
carbon with oxygen dominates the process. Possible interference effects
between the various reactants, and whether all the appropriate reactants
were considered also remains to be resolved.

Another variable of significant practical importance is the effect
of pressure. The present results were limited to atmospheric pressure
and whether the reaction expressions used here yield the proper pressure
dependence, must still be evaluated.

Appendix A

Computation of Properties

A.1 Mean Property State

The average properties of the gas surrounding the droplet were computed at the mean state, defined as follows:

$$\theta_{avg} = \alpha\theta_p + (1-\alpha)\ \theta_\infty \qquad (A-1)$$

where θ is a generic property at a specific temperature and mass fraction. α can range between 0 and 1 and a value of 0.9 was selected for the present investigation as suggested by Faeth and coworkers [9,10].

A.2 Mixture Thermal Conductivity

The thermal conductivity of the gaseous mixture was calculated with the Mason and Saxena formulation of the Wassiljewa equation [18].

$$\lambda_m = \sum_{i=1}^{N} \left[\frac{x_i \lambda_i}{\sum_{j=1}^{N} x_j \phi_{ij}} \right] \qquad (A-2)$$

where

$$\phi_{ij} = \frac{1}{8^{1/2}} \left(1 + \frac{M_i}{M_j}\right)^{-1/2} \left[1 + \left(\frac{\mu_i}{\mu_j}\right)^{1/2} \left(\frac{M_j}{M_i}\right)^{1/4}\right]^2 \qquad (A-3)$$

The thermal conductivity and viscosity for gases other than JP-10 was obtained from Ref. 19. The thermal conductivity of JP-10 was determined using the Miscic and Thodos method [18] and the viscosity of JP-10 was determined using the Reichenberg method [18]. Equation (A-2) was evaluated at the average temperature and composition of the gas phase. In Eq. (A-3), ϕ_{ij} is set equal to 1, when $i = j$.

A.3 Mixture Viscosity

The viscosity calculations for the mixture employed the method of Wilke, cited in Ref. 18.

For a mixture of N components

$$\mu_m = \sum_{i=1}^{N} \left[\frac{x_i \mu_i}{\sum_{j=1}^{N} x_j \phi_{ij}} \right] \tag{A-4}$$

where ϕ_{ij} is given by Eq. (A-3). The viscosity data used in the calculations was obtained in the same manner as described in Section A.2.

A.4 Mixture Diffusivity

When all of the liquid fuel has evaporated and only a carbon agglomerated particle remains the diffusion coefficient of the gas was taken for simplicity as the binary diffusion coefficient of oxygen through nitrogen

$$D = D_{O_2, N_2} \tag{A-5}$$

Use of other species combinations yielded diffusivities of similar magnitude.

References

1. G. W. Burdette, H. R. Lander and J. R. McCoy, "High Energy Density Fuels for Cruise Missiles," AIAA Paper No. 78-267 (1978).

2. T. W. Bruce, H. C. Mongia, R. S. Stearns, L. W. Hall and G. M. Faeth, "Formulation Properties and Combustion of Carbon-Slurry Fuels," Proceedings of Sixteenth JANNAF Combustion Meeting, CPIA Publication No. 308, pp. 679-717, December 1979.

3. T. W. Bruce and H. Mongia, "Compound Cycle Turbofan Engine Task IX: Carbon-Slurry Fuel Combustion Evaluation Program," Technical Report AFWAL-TR-80-2035, March 1980.

4. G. A. Szekely, Jr. and G. M. Faeth, "An Investigation of Slurry Fuel Combustion," Final Report to AiResearch Manufacturing Company of Arizona, Department of Mechanical Engineering, The Pennsylvania State University, November 1979.

5. R. H. Salvesen, "Carbon Slurry Fuels for Volume Limited Missiles," Technical Report AFAPL-TR-79-2122, November 1979.

6. R. S. Stearns, personal communication, June 20, 1979.

7. C. K. Law, C. H. Lee and N. Srinivasan, "Combustion Characteristics of Water-in-Oil Emulsions and Coal-Oil Mixtures," Paper No. 38, 1978 Technical Meeting, Eastern Section of the Combustion Institute, Miami Beach, FL, November 1978.

8. K. Miyasaka and C. K. Law, "Combustion and Agglomeration of Coal-Oil Mixtures in Furnace Environments," ASME Paper No. 80-HT-124 (1980).

9. C-P. Mao, G. A. Szekely, Jr. and G. M. Faeth, "Evaluation of a Locally Homogeneous Model of Spray Combustion," J. of Energy 4, 78-87 (1980).

10. A. J. Shearer, H. Tamura and G. M. Faeth, "Evaluation of a Locally Homogeneous Flow Model of Spray Evaporation," J. of Energy 3, 271-278 (1979).

11. G. M. Faeth, "Current Status of Droplet and Liquid Combustion," Prog. Energy Combust. Sci. 3, 191-224 (1977).

12. S. K. Ubhayakar and F. A. Williams, "Burning and Extinction of a Laser-Ignited Carbon Particle in Quiescent Mixtures of Oxygen and Nitrogen," J. Electrochem. Soc. 123, 747-756 (1976).

13. P. A. Libby and T. R. Blake, "Theoretical Study of Burning Carbon Particles," Combustion and Flame 36, 139-169 (1979).

References (Continued)

14. F. A. Williams, Combustion Theory, Addison-Wesley, Reading, MA, 1967.

15. N. M. Laurendau, "Heterogeneous Kinetics of Coal Char Gasification and Combustion," Prog. Energy Combust. Sci. 4, 221-270 (1978).

16. K. G. Neoh, J. B. Howard and A. F. Sarofim, "Soot Oxidation in Flames," Symposium on Particulate Carbon Formation During Combustion," G. M. Research Laboratories, Warren, MI, October 1980.

17. J. F. Johnstone, C. Y. Chen and D. S. Scott, "Kinetics of the Steam-Carbon Reaction in Porous Graphite Tubes," Ind. Engr. Chem. 44, 1564-1569 (1952).

18. R. C. Reid, J. M. Prausnitz and T. K. Sherwood, The Properties of Gases and Liquids, 3rd Edition, McGraw-Hill, New York, 1977.

19. R. A. Svehla, "Estimated Viscosities and Thermal Conductivities of Gases at High Temperatures," NASA-TR-132, 1962.

END

DATE
FILMED

4-8-1

DTIC